A Reconstructing Method for Multifeed Large-Scale Antenna Array Pattern Measurement

Peiqin Liu, *Student Member, IEEE*, Yue Li, *Senior Member, IEEE*, and Zhijun Zhang, *Fellow, IEEE*

***Abstract*—A far-field pattern reconstructing method is proposed for the multifeed large-scale antenna arrays in this paper. When the radiation pattern of a large-scale array is measured in the far field, the measurement distance is extremely large. To reduce the measurement distance, the conventional near-field measurement technique utilizes the near-field–far-field transformation to calculate the far-field radiation pattern. In this paper, the far-field pattern of multifeed large-scale antenna array is reconstructed at a given distance in the Fresnel region. In other words, the field distribution at the given distance matches well with the desired far-field pattern and can be directly measured by the far-field measurement technique. The far-field pattern reconstruction is realized by exciting the array elements with a specific phase distribution. The excitation strategy is determined by the given measurement distance and the direction of the far-field radiation pattern. Both theoretical and full-wave simulations are utilized to validate the proposed method. The results show that the measurement distance can be effectively reduced by using the proposed method. It should be noted that the proposed method is only studied and validated for a uniformly spaced point source array. The array is excited in phase or with a progressive phase distribution.**

***Index Terms*—Far-field pattern reconstruction, Fresnel region measurement, multifeed large-scale antenna array.**

I. Introduction

With the rapid development of wireless communication systems, multifeed large-scale antenna arrays are utilized in an increased number of applications. For example, massive MIMO, which is a key technique in the next generation of wireless communication systems, is a typical application of a multifeed large-scale antenna array [1], [2]. In a massive MIMO system, the antenna array generally has hundreds or even thousands of antenna elements and the aperture is quite large [3]–[5]. In terms of pattern measurements, there are some difficulties for multifeed large-scale antenna arrays. For pattern measurements, the near and far fields are defined in terms of the Fraunhofer distance. The distance is given as $2\,D^2/\lambda$, where D is the largest dimension of the array and λ is the wavelength in free space [6]. As a result, the Fraunhofer distance might be extremely large and measuring the radiation pattern of a large-scale array is quite difficult in the far-field region.

An effective method to reduce the measurement distance is using near-field measurements. The near-field–far-field (NF–FF) transformation technique has been widely investigated in recent decades [7]–[9]. Generally, a near-field measurement obtains far-field patterns by integrating all observation points on a Huygens surface [10]. Several methods have been proposed in the past few years to improve the performance of the NF–FF transformation. One method is optimizing scanning strategies, such as using plane-rectangular [10], plane-polar [12]–[14], bipolar [15]–[17], ϕ-variation [18], and spiral scanning [19], [20]. In addition to these scanning strategies, some researchers have investigated on optimizing the computational scheme of the NF–FF transformation [21]–[25]. In [21], a fast multilevel algorithm was proposed to reduce the memory requirements of the NF–FF transformation. The complex source beam method is a useful technique for predicting the scattering field from complex structures [22]. Fourier integrals at the Fresnel distances were utilized to determine far-field patterns in [23]. The source reconstruction method is another widely utilized technology [26]–[28]. This method samples near-field data to calculate an equivalent magnetic current source over a fictitious surface [26]. By utilizing the magnetic current source, the far fields can be obtained. All of the abovementioned methods are based on the NF–FF transformation technique, which samples observation points on a Huygens surface to calculate far-field patterns. However, by using the conventional NF–FF transformation technique, practical beam calibration is difficult for multibeam array applications [29].

In this paper, a far-field pattern reconstruction method is proposed for multifeed large-scale antenna arrays. Different from the conventional near-field measurement methods, the proposed method directly measures the far-field patterns at a given distance inside the Fresnel region without using the NF–FF transformation. The method is studied and validated for a uniformly spaced point source array, which is fed in phase or with a progressive phase distribution. The key process of the proposed method is exciting the antenna under test (AUT) with a specific phase distribution, which is associated with the measurement distance and the maximum radiation direction of the AUT. Table I compares the proposed method with the conventional measurement techniques. In far-field measurements, the source antenna should be located in the Fraunhofer region, and the measurement distance would be quite large for a large-scale antenna array. The NF–FF transformation technique can effectively

Manuscript received May 2, 2018; revised September 15, 2018, November 14, 2018, and December 19, 2018; accepted December 21, 2018. Date of publication December 28, 2018; date of current version January 18, 2019. This work was supported in part by the National Natural Science Foundation of China under Contract 61525104 and in part by the Natural Science Foundation of Beijing Municipality under Contract 4182029. *(Corresponding author: Zhijun Zhang.)*

The authors are with the Beijing National Research Center for Information Science and Technology, Tsinghua University, Beijing 100084, China (e-mail: lpq14@mails.tsinghua.edu.cn; lyee@tsinghua.edu.cn; zjzh@tsinghua.edu.cn).

Digital Object Identifier 10.1109/JMMCT.2018.2890107

TABLE I
QUALITY COMPARISONS

Technique / Property	Far-Field Measurement	NF-FF Transformation	Proposed Method
Measurement Distance	Fraunhofer Region	Fresnel Region	Fresnel Region
Probe Scanning	No	Yes	No
Measurement Time	Short	Long	Short
Phase Compensation	No	No	Yes
Accuracy	Highest	High	Slight errors

reduce the measurement distance from the Fraunhofer region to the Fresnel region. However, the NF–FF transformation is based on probe scanning, which spends an appreciable amount of time sampling on a Huygens surface to compute the far-field pattern. In addition, the phase calibration in the NF–FF transformation is difficult for a multifeed antenna array. In the proposed method, the far-field pattern is reconstructed and directly measured in the Fresnel region by phase compensation. As a result, the measurement time is the same as that of a conventional far-field measurement. In fast testing applications, this property is quite significant. When a batch of large-scale antenna arrays is under test, the fastest way to examine their radiation performance is to check the consistency of the maximum gain. In [26], a 32 × 32 patch microstrip array with broadside radiation was measured using the NF–FF transformation. To compute the far fields, 8100 discrete points are measured in this method. In other words, the method needs 8100 measurements to obtain the gain in the broadside direction. In the proposed method, the far-field pattern is reconstructed in the Fresnel region without using the NF–FF transformation. One can directly measure the gain in the broadside direction with a one-time measurement. It should be noted that there are some errors in the proposed method. The errors are relatively slight and occur in regions away from the main beam. The results in the region of the main beam are accurate. Both theoretical and full-wave simulations are utilized to validate the proposed far-field pattern reconstructing method. The results demonstrate that the proposed method has high potential in multifeed large-scale antenna array measurement applications.

II. ANALYSIS OF A ONE-DIMENSIONAL (1-D) ARRAY

In this section, a uniformly excited linear array is utilized to analyze the proposed method. Moreover, the proposed method can be extended to the 2-D planar array as shown in later sections.

A. Excitation Strategy of the Proposed Method

The configuration of the uniformly excited N-element linear array is shown in Fig. 1 in relation to the coordinate system. All the point sources are excited in phase. The angle φ is measured counterclockwise from the positive *X*-coordinate. The spacing between adjacent point sources is $d = \lambda/2$, where λ is the wavelength in free space. For far-field measurements, as depicted in Fig. 1(a), the distance difference between adjacent elements is $d\cos\varphi$. The phase difference is $\beta d\cos\varphi$, where β is the phase

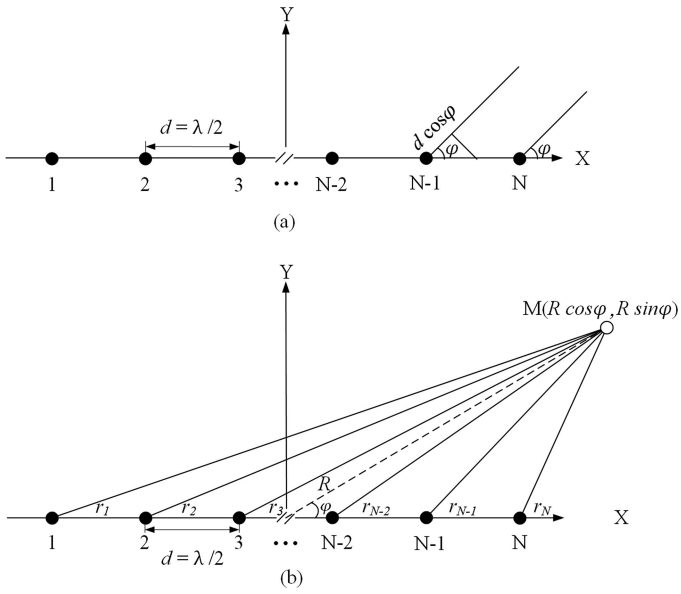

Fig. 1. Isotropic point sources in a uniformly excited N-element linear array. (a) Observe in the far-field region. (b) Observe in the Fresnel region.

constant in free space and $\beta = 2\,\pi/\lambda$. In the Fraunhofer region, the phase difference is independent of the measurement distance *R*. However, when the array is measured in the Fresnel region, the phase difference between adjacent elements is associated with the measurement distance. As shown in Fig. 1(b), point M represents the measurement point in the Fresnel region. The distance between the point M and the original point is *R*. The angle φ is measured counterclockwise from the positive *X*-coordinate to the point M. The distance $r_i (i = 1, 2, \ldots, N-1, N)$ is the distance between the point M and the *i*th point source. Thus, r_i can be calculated as

$$r_i = \sqrt{(R\cos\varphi - x_i)^2 + (R\sin\varphi)^2}, (i = 1, 2, \ldots, N-1, N) \tag{1}$$

where x_i is the position of the *i*th point source in the *X*-coordinate, and x_i can be expressed as

$$x_i = d\left(i - \frac{N+1}{2}\right)(i = 1, 2, \ldots, N-1, N). \tag{2}$$

As a result, the phase difference between adjacent elements, i.e., the *i*th element and the $(i+1)$th element, is

$$\text{PhaseDiff}_{i,i+1} = 2\pi\frac{(r_i - r_{i+1})}{\lambda}(i = 1, 2, \ldots, N-1). \tag{3}$$

Substituting (1) into (3), one can find that the phase difference between adjacent elements is associated with the measurement distance *R* and the angle φ.

B. Example of a Uniform 20-Element Linear Array

To describe the phase difference more clearly, a linear array with 20 elements is proposed as an example. Fig. 2 shows the phase difference between adjacent elements in the 20-element array. Fig. 2(a) shows the phase difference in the far-field range. Since the spacing, *d* is $\lambda/2$, the phase difference $\beta d\cos\varphi$ equals

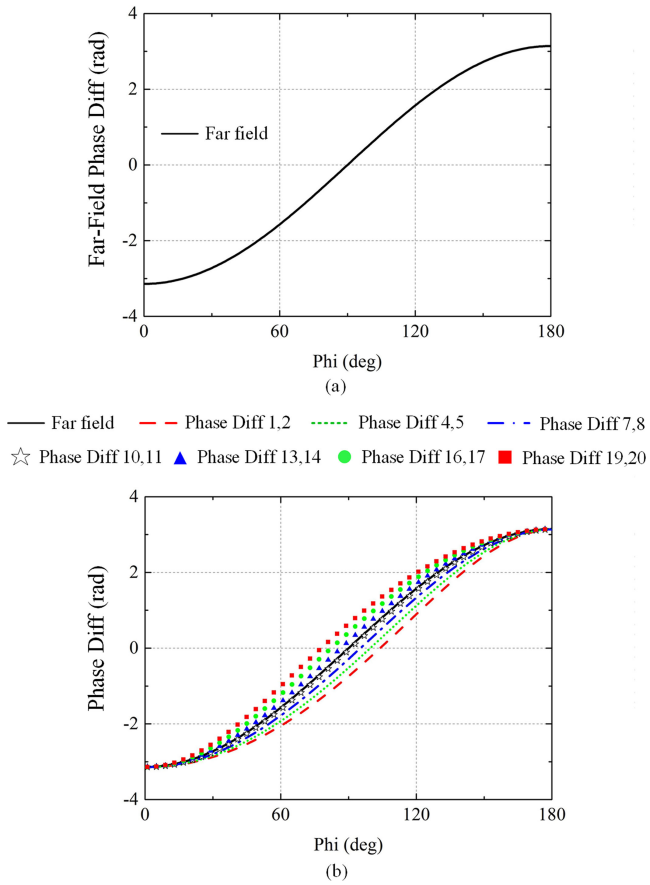

Fig. 2. Phase difference between adjacent elements of a 20-element linear array. (a) Observe in far-field region. (b) Observe in the Fresnel region at distance $R = 20\lambda$.

to $\pi\cos\varphi$. As a result, the far-field phase difference between adjacent elements is identical and the phase difference is plotted in Fig. 2(a). According to the function of $2D^2/\lambda$, where D is the largest dimension of the array, the Fraunhofer distance of the 20-element linear array is approximately 200λ. For a given distance in the Fresnel region, such as $R = 20\lambda$, the phase differences between adjacent elements are plotted in Fig. 2(b). In the 20-element array, there are 19 pairs of adjacent elements, which correspond to 19 phase differences. In Fig. 2(b), the phase differences are plotted for every third one for simplicity. Compared with the phase difference in the far-field region, the phase difference in the Fresnel region is associated with the positions of the point sources, and they are quite different from the far-field phase difference. As shown in Fig. 2(b), when $\varphi = 0°$, all of the phase differences are equal to $-\pi$ and there is no difference between the far-field region and the Fresnel region. As the angle φ increases, the difference increases and the largest difference occurs at $\varphi = 90°$, i.e., the maximum radiation direction of an in-phase linear array. As the angle further increases, the difference decreases and achieves the smallest difference once again at the end-fire direction of $\varphi = 180°$. In this direction, all of the phase differences are π.

The parameter $\text{PhaseDiffi}_{i,i+1}$ is the phase difference between the ith element and the $(i+1)$th element. Since $\text{PhaseDiffi}_{i,i+1}$ is obtained in the Fresnel region, there are phase difference errors between $\text{PhaseDiffi}_{i,i+1}$ and the far-field phase difference. Fig. 2(b) shows that the $\text{PhaseDiffi}_{1,2}$ and the $\text{PhaseDiff}_{19,20}$ have the largest phase difference error with respect to the phase difference in the far-field region. Moreover, at the angle of $\varphi = 90°$, the phase difference error is maximum. Considering that the maximum radiation direction of an in-phase linear array also points at the angle of $\varphi = 90°$, the phase difference error greatly affects the measured results.

To mitigate the phase difference error, an excitation strategy is proposed in this paper. For a 20-element linear array as shown in Fig. 3(a), the excitation strategy is obtained as follows. At first, the measurement point M is located in the maximum radiation direction of the array, i.e., with an angle of $\varphi = 90°$, and the measurement distance from point M to the original point is R. Second, substitute $\varphi = 90°$ and the distance R into (1) to obtain the distance $r_i (i = 1, 2, \ldots, 19, 20)$ from the ith point source to the measurement point M. Finally, based on the distances r_i, the compensating phase of the ith point source can be calculated as

$$\alpha_i = 2\pi \frac{r_i}{\lambda}, (i = 1, 2, \ldots, 20). \tag{4}$$

The phase compensations for the array elements are plotted in Fig. 3(b). Since the first element and the last element have the largest distance to the measurement point, they have the largest compensating phase. Similarly, the 10th element and the 11th element have the smallest compensating phase. Based on the compensation phase, the phase difference from the array elements to the measurement point can be recalculated. The phase differences between adjacent elements of the proposed method are plotted in Fig. 3(c). By utilizing the proposed excitation strategy, the phase difference error is zero at the maximum radiation direction of $\varphi = 90°$. As the angle φ varies to the end-fire directions, the error increases, and the largest error occurs at angles of $\varphi = 0°$ and $\varphi = 180°$. However, for pattern measurements, the most significant data are the results around the maximum radiation direction. Because the phase difference errors in the maximum radiation direction are quite trivial, the proposed method could precisely reconstruct the main beam of the far-field pattern. In regard to the end-fire directions, the directivity of the far-field pattern is quite low. Although the phase difference errors are relatively large, the phase-difference error would slightly affect the results at those angles.

As shown in Fig. 4, theoretical pattern analyses are proposed to study the effect of the proposed method. There are three patterns in Fig. 4. These patterns include the far-field pattern, the Fresnel field, which is directly measured at the Fresnel distance, and the field of the proposed method. To measure the array in the far-field region, the measurement distance should be larger than 200λ. In the ideal far-field pattern, the maximum directivity is 13.01 dBi at an angle of $\varphi = 90°$, and the first side-lobe level (SLL) is -13.19 dB. The field in the Fresnel region is calculated at different distances of $R = 20\lambda$, 40λ, and 60λ. When the in-phase linear array is directly measured in the Fresnel region, the pattern deteriorates due to phase errors. Fig. 4 shows that at distances of $R = 20\lambda$, 40λ, and 60λ, the maximum directivities of the Fresnel field are 6.74, 11.50, and 12.33 dBi, respectively. Compared with the far-field pattern, the maximum directivity decreases by 5.66, 1.51, and 0.68 dB, respectively. Moreover, the SLL also deteriorates due to the phase error. When the

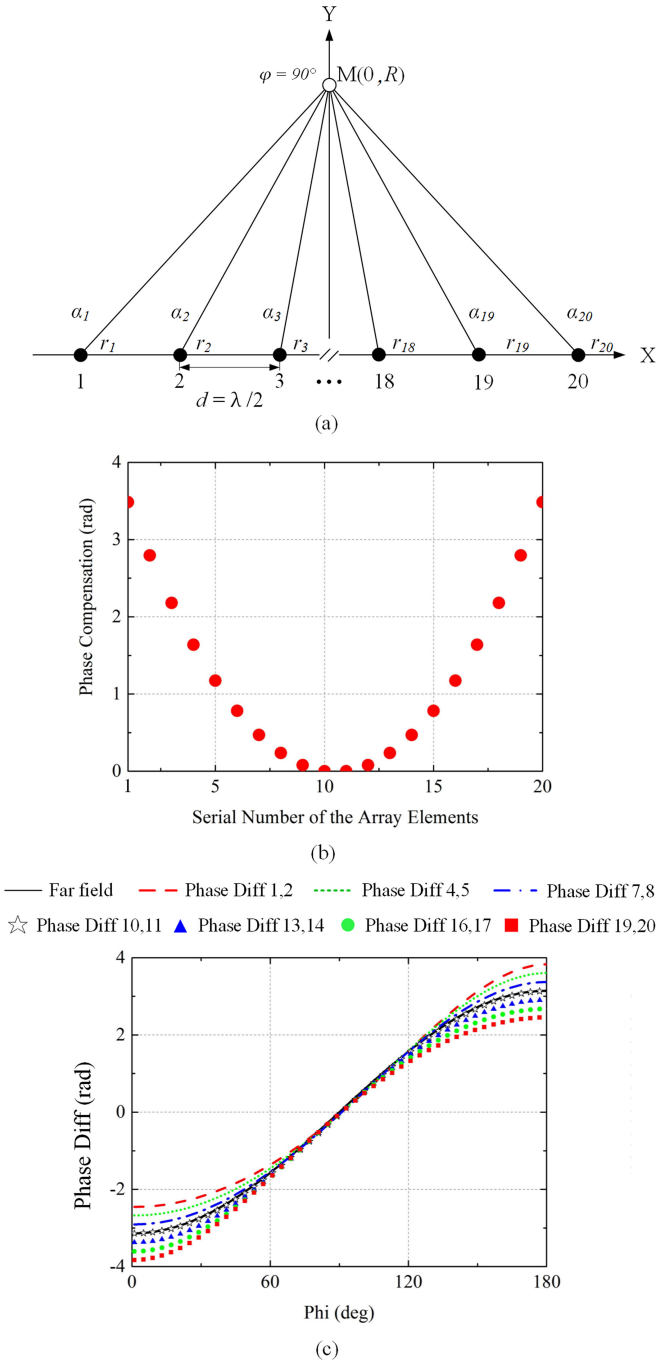

Fig. 3. Twenty-element array measured in the Fresnel region. (a) Schematic of the proposed method. (b) Phase distribution of the proposed method. (c) Phase difference between adjacent elements at distance $R = 20\lambda$.

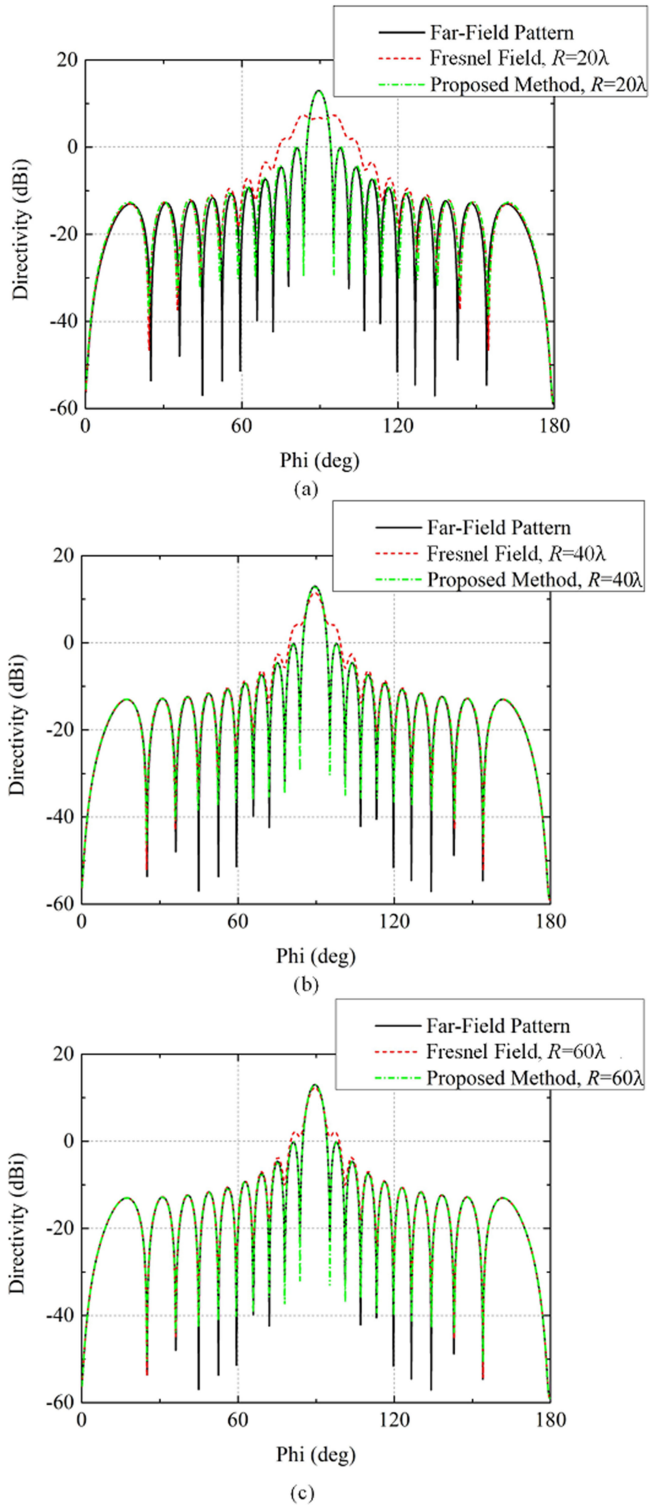

Fig. 4. Radiation pattern and field of a uniformly excited 20-element array. The theoretical field in the Fresnel region is calculated in different distances of (a) $R = 20\lambda$, (b) $R = 40\lambda$, and (c) $R = 60\lambda$.

array is directly measured at a distance of $R = 20\lambda$, the SLL deteriorates considerably, and the grating lobes appear. As the measurement distance increases to $R = 40\lambda$ and 60λ, the first SLLs are -7.34 and -10.17 dB, respectively. Compared with the far-field pattern, the first SLL increases by 5.85 and 3.02 dB, respectively.

By utilizing the proposed method, the errors can be effectively mitigated. The field of the proposed method is illustrated in Fig. 4 for comparison. The measurement distance is also located in the Fresnel region at distances of $R = 20\lambda, 40\lambda$, and 60λ. Fig. 4 shows that the results of the proposed method match well with the far-field patterns. The error decreases as the measurement distance increases. Even for the smallest measurement distance, i.e., $R = 20\lambda$, the maximum directivity error and the first SLL error are less than 0.5 dB in the proposed method. The detailed results are listed in Table II for comparison.

TABLE II
DETAILED RESULTS

	Far Field Pattern	Fresnel Field	Proposed Method
Directivity (R=20λ)	13.01 dBi	6.74 dBi	12.86 dBi
Directivity (R=40λ)	13.01 dBi	11.50 dBi	12.87 dBi
Directivity (R=60λ)	13.01 dBi	12.33 dBi	12.89 dBi
1st SLL (R=20λ)	-13.19 dB	+0.61 dB	-12.70 dB
1st SLL (R=40λ)	-13.19 dB	-8.46	-13.04 dB
1st SLL (R=60λ)	-13.19 dB	-10.68 dB	-13.12 dB

In addition to the measurement distance, the number of array elements is another key parameter that affects the measurement results in the Fresnel region. Fig. 5 shows theoretical analyses of the linear array with different element numbers. The Fresnel field and the field of the proposed method are obtained in the Fresnel region at a distance of $R = 60\lambda$. Fig. 5 shows that when the number of array elements increases, the directly measured Fresnel field deteriorates and the grating lobes increase. The results of the proposed method still match well with the far-field pattern. Detailed results are listed in Table III for comparison.

C. Analysis of Phase Error

The proposed method utilizes phase compensation to reconstruct far-field patterns. The performance of the method relies on the accuracy of the phase delay from the measurement point M to each radiation element. An analysis of phase error is proposed in this section. The analysis is based on a uniformly excited 20-element linear array, which is the same as the array in Fig. 4(b). Random phase errors are introduced into each radiation element and the results are illustrated in Fig. 6. In Fig. 6(a), the array has a 5-bit phase error, which is limited to $\pm 11.25°$. The results are obtained as follows. At first, 20 phase errors are randomly generated from $-11.25°$ to $+11.25°$. Second, the phase errors are added to each radiation element so that the field of the proposed method can be obtained with the phase error. Then, the first and the second steps are repeated 100 times to obtain 100 different radiation patterns. Finally, the maximum and minimum values at every angle are plotted in Fig. 6(a) to show the influence of the phase error. In Fig. 6(b) and (c), the results are obtained with the same method and the phase errors are limited to $\pm 5.625°$ (6 bit) and $\pm 2.8125°$ (7 bit), respectively. Fig. 6 illustrates that the phase error influences the side lobes. The main beam would not be affected by the phase error. Moreover, from Fig. 6(a)–(c), one can observe that as the limitation of phase errors decreases from 5-bit phase error to 7-bit phase error, the influence of the phase errors also decreases. In practical applications, a T/R module with a high-accuracy phase shifter could be used to improve the performance of the proposed method.

D. Example of a 20-Element Array With a Dolph–Chebyshev distribution

The abovementioned analyses are based on a uniformly excited linear array. For some applications, a nonuniform amplitude distribution is utilized to reduce the SLL. In this section, a

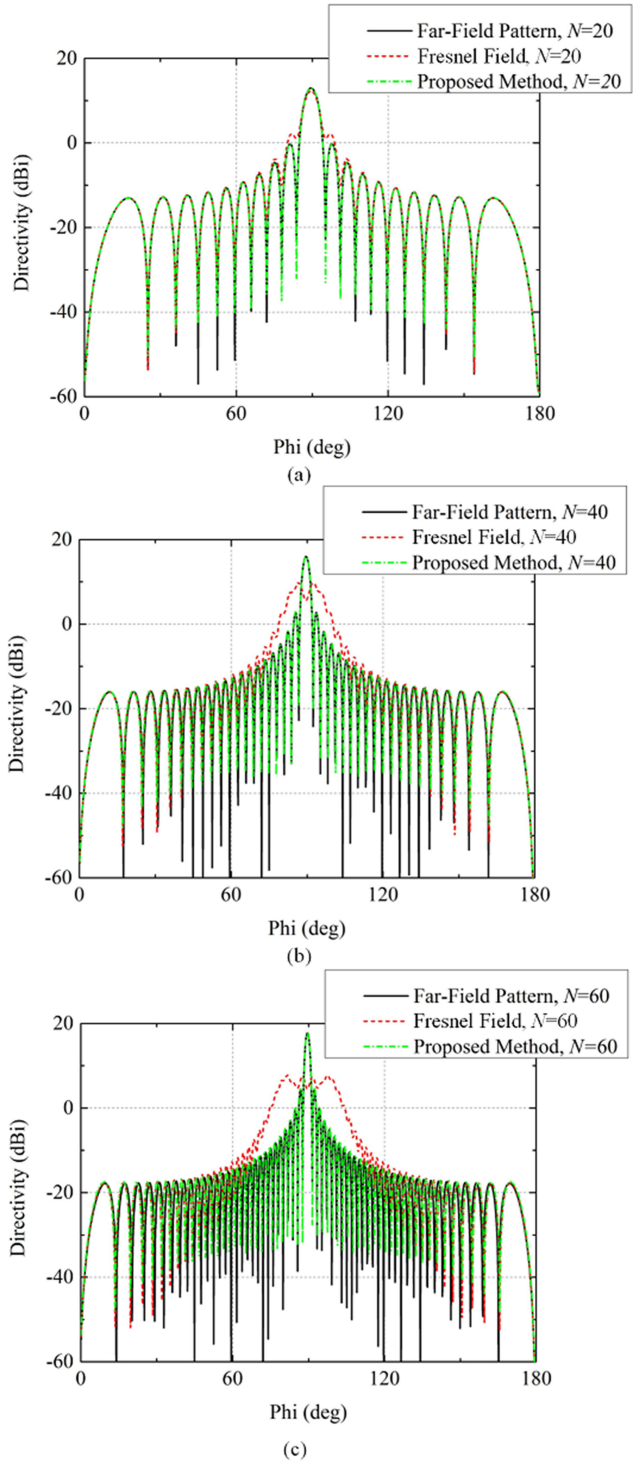

Fig. 5. Radiation pattern and field of uniformly excited linear arrays with different numbers of elements. (a) Number $N = 20$, (b) Number $N = 40$, and (c) Number $N = 60$. All of the results are calculated at the measurement distance $R = 60\lambda$ in the Fresnel region.

20-element array with the Dolph–Chebyshev (D-T) distribution [30] is analyzed. Fig. 7 shows the radiation pattern results. All the results are obtained with the D-T distribution. The SLL in the far-field pattern is lower than -30 dB. The Fresnel field is directly measured at a distance of $R = 40\lambda$. One can observe that the maximum directivity decreases by 1.0 dB in the Fresnel field. Moreover, the beam width and SLL are also distorted. In

TABLE III
DETAILED RESULTS

	Far Field Pattern	Fresnel Field	Proposed Method
Directivity (N=20)	13.01 dBi	12.33 dBi	12.89 dBi
Directivity (N=40)	15.64 dBi	5.87 dBi	15.59 dBi
Directivity (N=60)	16.95 dBi	4.87 dBi	16.84 dBi
1st SLL (N=20)	-13.19 dB	-10.68 dB	-13.12 dB
1st SLL (N=40)	-13.78 dB	+3.82 dB	-13.38 dB
1st SLL (N=60)	-12.94 dB	+2.94 dB	-12.76 dB

the proposed method, the amplitude distribution is based on the D-T distribution and the compensating phase is the same as in the abovementioned uniform array. As shown in Fig. 7, the field of the proposed method matches well with the far-field pattern and the error in the first SLL is only 0.1 dB.

III. Analysis of a 2-D Planar Array

A. Excitation Strategy of the Proposed Method

Similar to the 1-D array, the proposed method can be extended to 2-D arrays. The configuration of a uniformly excited N-by-N array is shown in Fig. 8 in relation to the coordinate system. The spacing distance between adjacent point sources is λ/2. The location of the ith point source is (X_i, Z_i) $(i = 1, 2, \ldots, N^2 - 1, N^2)$, where X_i is the address of the ith point source in the X-coordinate, and Z_i is the address in the Z-coordinate. The distance $r_i (i = 1, 2, \ldots, N^2 - 1, N^2)$ is the distance from the measurement point M (R, θ, φ) to the ith point source in the 2-D array. As a result, r_i can be calculated as

$$r_i = \sqrt{(R\sin\theta\cos\varphi - X_i)^2 + (R\sin\theta\sin\varphi)^2 + (R\cos\theta - Z_i)^2} \tag{5}$$

where i is the index of the point sources, and $i = 1, 2, \ldots, N^2 - 1, N^2$.

For an in-phase planar array, the maximum directivity direction is the broadside direction at the angle of $\theta = 90°$ and $\varphi = 90°$. At a given distance R inside the Fresnel region, the compensating phase of the proposed method is

$$\alpha_i = 2\pi\frac{r_i}{\lambda}, (i = 1, 2, \ldots, N^2 - 1, N^2). \tag{6}$$

As an example, a 20-by-20 planar array is utilized to analyze the proposed method. The planar array is located in the xz plane. Fig. 9 depicts the 3-D radiation pattern and field in the upper space. Fig. 9(a) shows the far-field pattern of the 20-by-20 planar array. The point sources in the planar array are excited in-phase. The maximum directivity is 27.9 dBi in the broadside direction and the first SLL is −13.3 dB. Fig. 9(b) illustrates that if the field is directly measured at a distance of $R = 40\lambda$, the results deteriorate substantially. In Fig. 9(b), the maximum directivity is 24.8 dBi and the first SLL is −7.3 dB. Compared with the far-field pattern, the maximum directivity decreases by

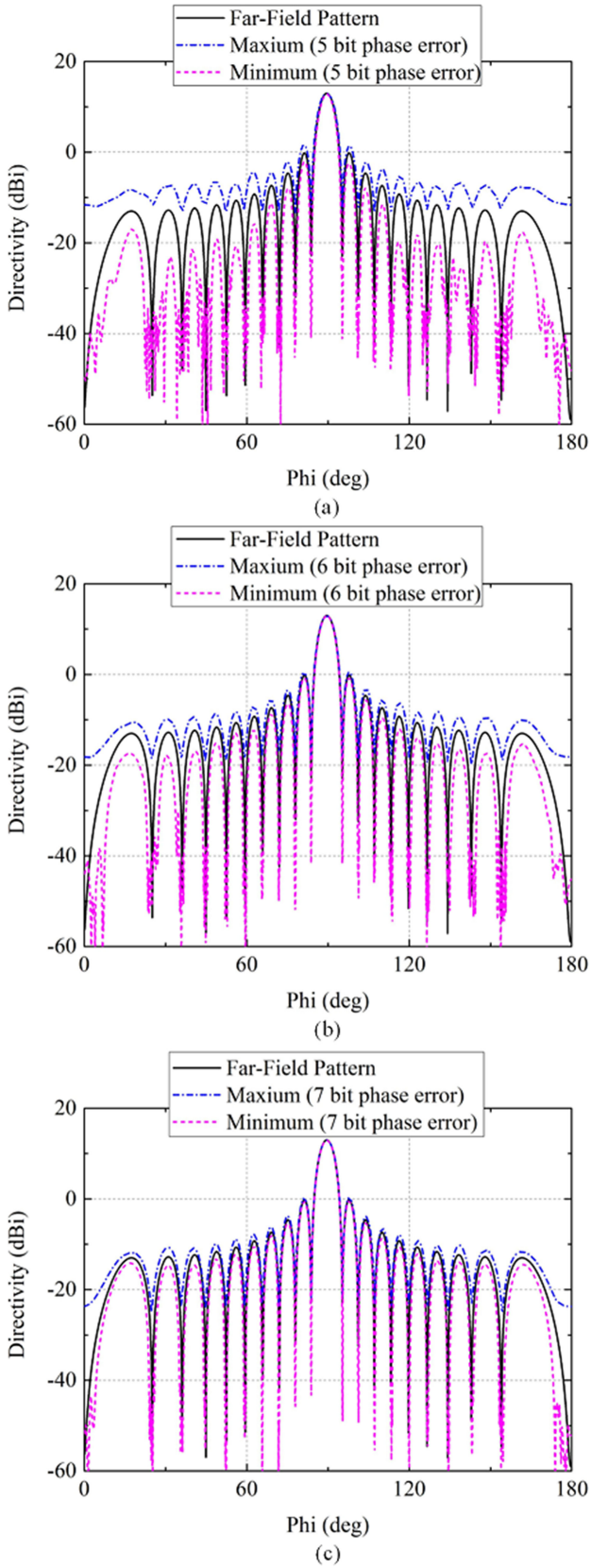

Fig. 6. Radiation patterns of the proposed method with different levels of phase error. (a) 5-bit phase error, which is limited within ±11.25°, (b) 6-bit phase error, which is limited within ±5.625°, and (c) 7-bit phase error, which is limited within ±2.8125°. All of the patterns are calculated based on a uniformly excited 20-element linear array at distance $R = 40\lambda$ in the Fresnel region.

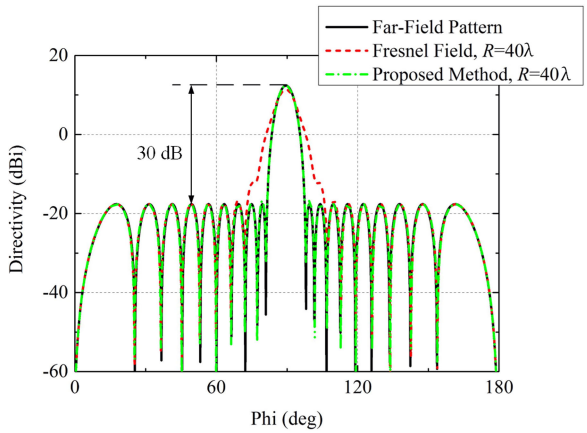

Fig. 7. Radiation patterns of a 20-element array with Dolph–Chebyshev distribution.

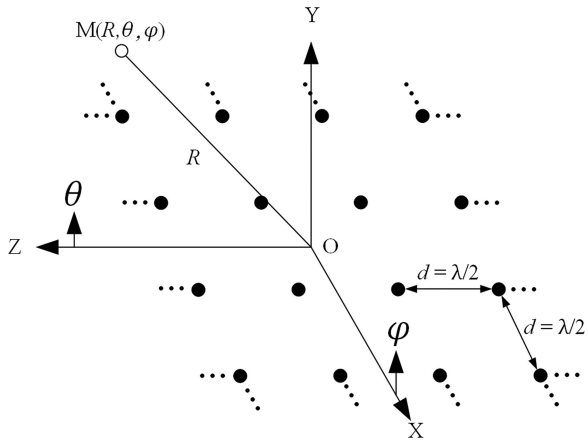

Fig. 8. Isotropic point sources in a uniformly excited N-by-N 2-D planar array.

3.1 dB, and the first SLL increases by 6.0 dB. Fig. 9(c) depicts the result of the proposed method. One can observe that the field of the proposed method matches well with the far-field pattern. The maximum directivity in Fig. 9(c) is 27.8 dBi, which is only 0.1 dB lower than the far-field pattern. The first SLL is −13.3 dB, which is the same as that of the far-field pattern.

To show the effect of the proposed method more quantitatively, Fig. 10 depicts the errors for different measurement methods. Fig. 10(a) shows the errors between the Fresnel field and the far-field pattern. The maximum error is 16.8 dB, and it occurs at the first null of the far-field pattern. Fig. 10(b) shows the errors between the result of the proposed method and the far-field pattern, and the maximum error in Fig. 10(b) is only 1.5 dB. The results demonstrate that the proposed method can effectively reconstruct the far-field pattern at a given distance inside the Fresnel region.

It should be noted that the errors in Fig. 10 are not calculated by directly subtracting the patterns in Fig. 9. When the maximum directivity and the side lobes are subtracted, the errors can be calculated precisely. However, in regard to the nulls of the radiation pattern, directly subtracting the values of the nulls might introduce meaningless results. For example, in Fig. 9(a),

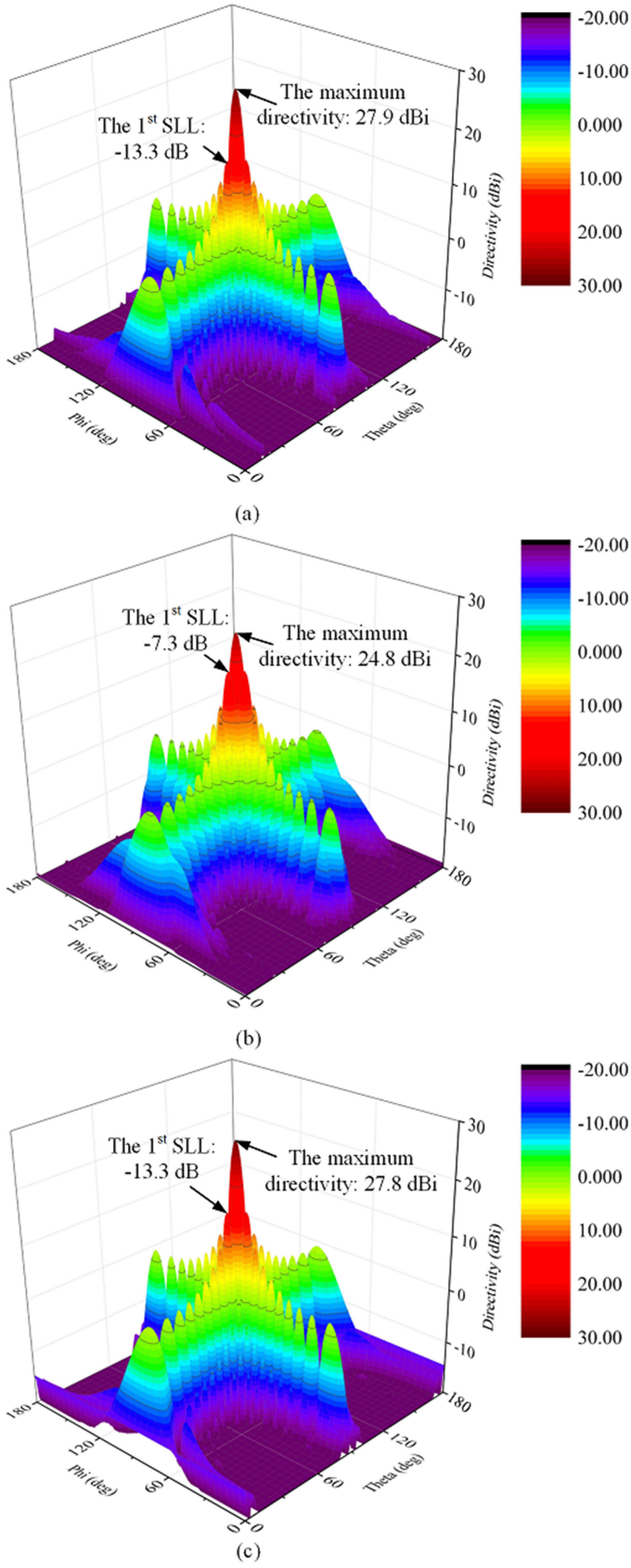

Fig. 9. Three-dimensional radiation patterns in upper space. The planar array is a uniformly excited 20-by-20 planar array with broadside radiation. (a) Far-field pattern. (b) Pattern in the Fresnel region at distance of $R = 40\lambda$. (c) Pattern of the proposed method in the Fresnel region at distance of $R = 40\lambda$.

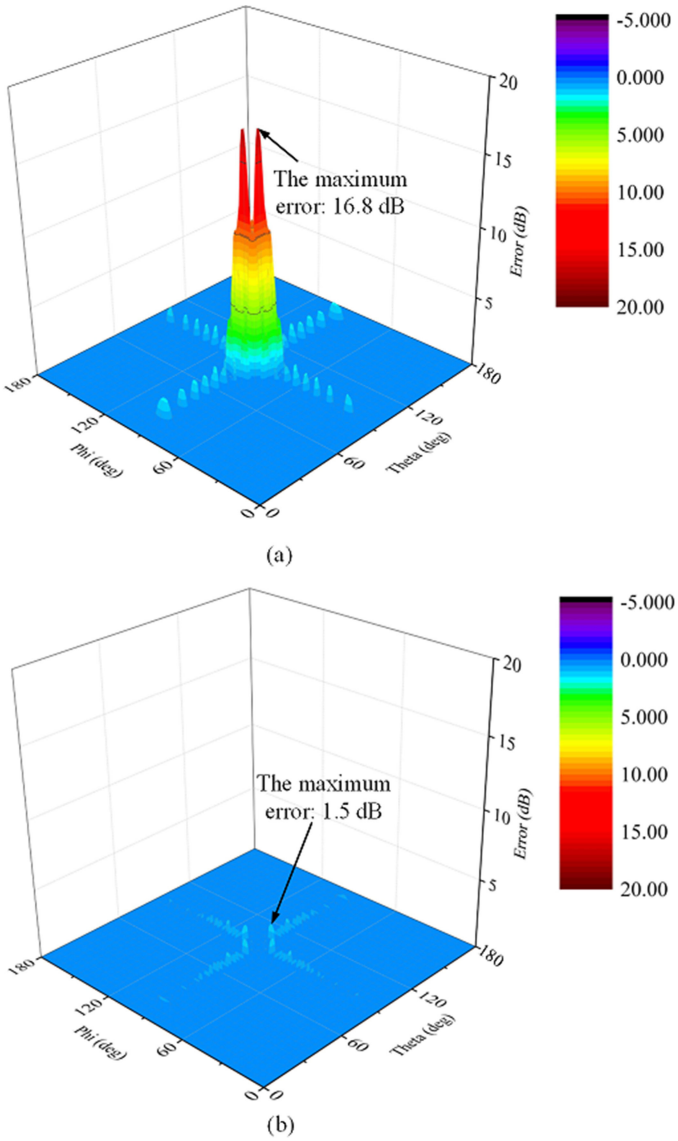

Fig. 10. Pattern errors of the 20-by-20 broadside planar array. (a) Errors between far-field pattern and the Fresnel pattern. (b) Errors between far-field pattern and the pattern of proposed method.

the pattern is null at the angle of $\theta = 90°$ and $\theta = 60°$, and the directivity is -48.0 dBi, which is 75.9 dB lower than the maximum directivity. At the same angle as that in Fig. 9(c), the directivity is -13.3 dBi, which is 41.1 dB lower than the maximum directivity. The value in Fig. 9(c) is small enough to be considered as a null. However, if the two patterns are subtracted directly, the error will be 34.7 dB, which is an extremely high error that is not reasonable. Therefore, the values in the patterns are preprocessed, which leads to values lower than 0 dBi and makes them equal to 0 dBi. Then, the processed patterns are subtracted to obtain the errors in Fig. 10.

The errors can be expressed as

$$\begin{aligned} F_1' &= \max(F_1, 0\,\text{dBi}) \\ F_2' &= \max(F_2, 0\,\text{dBi}) \\ F_3' &= \max(F_3, 0\,\text{dBi}) \end{aligned} \tag{7}$$

where F_1, F_2, and F_3 are the array factors of the far-field pattern, the Fresnel field, and the proposed method, respectively.

$$\begin{aligned} \text{Error}_1 &= abs(F_2' - F_1') \\ \text{Error}_2 &= abs(F_3' - F_1') \end{aligned} \tag{8}$$

where Error_1 is the error between the far-field pattern and the Fresnel field as shown in Fig. 10(a) and Error_2 is the error between the far-field pattern and the proposed method as shown in Fig. 10(b).

B. Strategy for an Array With Different Radiation Directions

The abovementioned analyses are proposed for an in-phase planar array, which points to the broadside direction. If the array is excited with a progressive phase distribution, the radiation direction would be steered to different directions. This section validates that the proposed method can be extended to an array with a progressive phase distribution.

For a planar array radiating in the direction of angle (θ_m, φ_m), the phase compensation of the proposed method can be obtained by substituting the values θ_m and φ_m into (5) and (6).

For example, a 20-by-20 planar array is illustrated in Fig. 11 with a radiation direction at the angle of $\theta = 90°$, $\varphi = 60°$, which is tilted 30° away from the broadside direction. Fig. 11(a) shows the far-field pattern of the planar array. The maximum directivity is 27.2 dBi, and the first SLL is -13.2 dB. Fig. 11(b) shows the Fresnel field at a distance of $R = 40\lambda$ inside the Fresnel region. Since the measurement distance cannot satisfy the far-field condition, the field in Fig. 11(b) deteriorates. The maximum directivity is 24.8 dBi and the first SLL is -10.1 dB. Compared with the far-field pattern in Fig. 11(a), the maximum directivity decreases by 2.4 dB and the first SLL increases by 3.1 dB. Fig. 11(c) shows the result of the proposed method, in which the array is excited with the phase distribution of the proposed method and the field is also measured at a distance of $R = 40\lambda$. The maximum directivity in Fig. 11(c) is 27.1 dBi and the first SLL is -13.1 dB. Compared with the far-field pattern in Fig. 11(a), the errors in the maximum directivity and the first SLL are 0.1 dB, which demonstrate the effectiveness of the proposed method.

Similar to the errors shown in Fig. 10, the error of the proposed method is shown in Fig. 12. The errors are also calculated based on (7) and (8). Fig. 12(a) shows that the maximum error between the Fresnel field and the far-field pattern is 16.8 dB, which occurs at the first null of the far-field pattern. Fig. 12(b) shows the errors between the proposed method and the far-field pattern. The maximum error of the proposed method is 1.5 dB.

C. Relationship Between Element Number and Measurement Distance

In the proposed method, the far-field pattern is reconstructed at a given distance R inside the Fresnel region. The measurement distance can be arbitrarily chosen in the theoretical analysis. In practical applications, the relationship between the array aperture and measurement distance is significant. This demonstrates the size requirement for an anechoic chamber when a multifeed

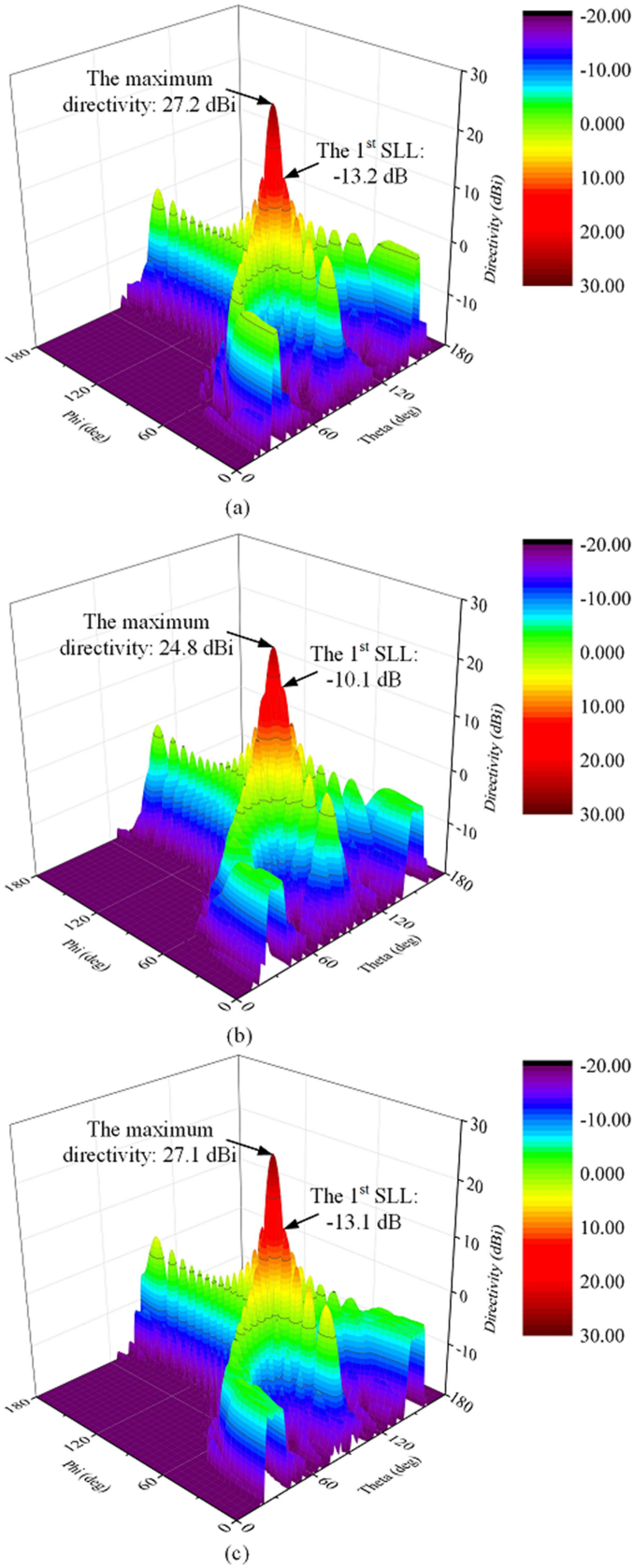

Fig. 11. Three-dimensional radiation patterns in upper space. The planar array is a 20-by-20 planar array with radiation direction at angle of $\theta = 90°$, $\varphi = 60°$. (a) Far-field pattern. (b) Pattern in the Fresnel region at distance of $R = 40\lambda$. (c) Pattern of the proposed method in the Fresnel region at distance of $R = 40\lambda$.

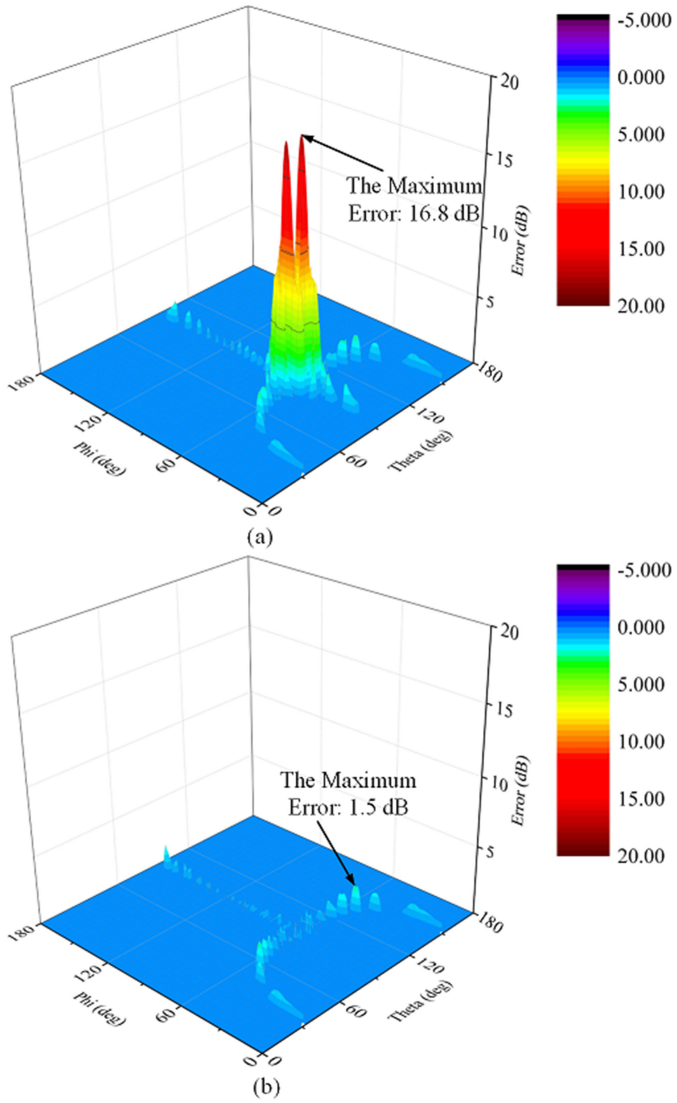

Fig. 12. Pattern errors of the 20-by-20 planar array. The radiation direction is at the angle of $\theta = 90°$ and $\varphi = 60°$. (a) Errors between far-field pattern and the Fresnel field. (b) Errors between far-field pattern and the result of the proposed method.

large-scale antenna array is measured. Fig. 13 shows the relationship between element number and measurement distance for an in-phase N-by-N planar array. The maximum directivity difference between the far-field pattern and the field of the proposed method is utilized as a criterion to determine the measurement distance. The line plotted with solid squares is the maximum directivity difference, which is less than 0.1 dB between the far-field pattern and the field of the proposed method. For the line plotted with solid circles, the difference is less than 0.3 dB. The Fraunhofer distance is also depicted as a reference in Fig. 13 by the line plotted with solid triangles. Fig. 13 shows that the proposed method becomes more effective as the array aperture size increases. For example, the Fraunhofer distance of a 40-by-40 planar array is 1600λ. Using the proposed method, the measurement distance can be reduced to 80λ with an error of less than 0.1 dB or 45λ with an error of less than 0.3 dB. In practical applications, when an antenna array is measured with the

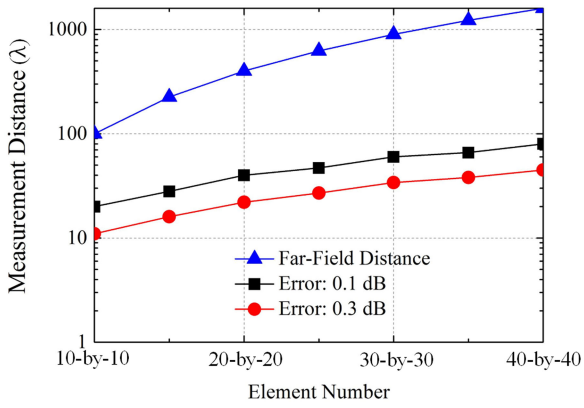

Fig. 13. Relationship between element number and measurement distance.

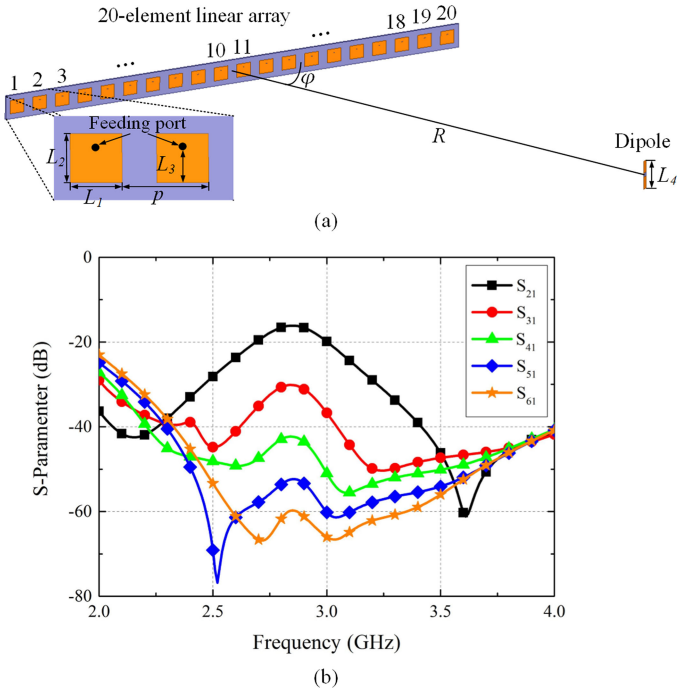

Fig. 14. Full-wave analysis of the proposed method. (a) HFSS model configuration for measuring a 1-D 20-element array. Detailed dimensions: $L_1 = 30$ mm, $L_2 = 28$ mm, $L_3 = 20$ mm, $L_4 = 47$ mm, and $p = 50$ mm. The measurement distance in the Fresnel region is $R = 4000$ mm. (b) Isolation between radiation elements.

proposed method, users can check Fig. 13 as a reference to find a suitable measurement distance based on the array aperture and the error criterion. On the other hand, if an anechoic chamber already exists, which means the maximum measurement distance is given, users can check Fig. 13 to find the largest antenna array aperture that can be measured in the anechoic chamber.

IV. Numerical Results

To verify the far-field pattern reconstructing method, a full-wave simulation is proposed in this section. The FEBI radiation boundary of ANSYS high frequency structure simulator (HFSS) version 15 is utilized in the simulation. Due to the limitation of computing resources, a uniformly excited 20-element 1-D linear array is simulated as an AUT. Fig. 14(a) shows the configuration and detailed dimensions of the HFSS model. The linear array contains 20 patch antennas and operates at 2.84 GHz. The patch array is designed based on an F4b substrate ($\varepsilon_r = 2.65$) with a thickness of 1 mm. Every patch antenna is excited through an independent port. A dipole antenna, which acts as a source antenna, is located in the Fresnel region of the 20-element array. In the proposed HFSS model, the measurement distance R is approximately 40λ from the center of the patch array to the dipole. At first, the dipole antenna is located in the direction of $\varphi = 90°$. The transmission coefficients, including both magnitude and phase, from every patch element to the dipole can be obtained through simulation. By using the transmission coefficients, one can calculate the total electric field received by the dipole antenna. Then, one can rotate the dipole antenna with different values of φ and calculate the total electric field at different angles. By utilizing these data, the Fresnel field and the field of the proposed method can be calculated.

It should be noted that the mutual coupling between radiation elements should be relatively low in the proposed method. Thus, the current distribution is well localized to the element and the element phase pattern is constant in the region of interest. Fig. 14(b) shows the mutual coupling between the radiation elements. For simplicity, five curves are selected to show the variation regularity. One can observe that all of the mutual coupling curves are lower than -16 dB. The highest mutual coupling occurs between two adjacent elements, i.e., S_{21}. As the distance increases, the mutual coupling decreases.

Fig. 15 shows the full-wave simulation results. Fig. 15(a) illustrates the simulated pattern and field. The far-field pattern is directly simulated by HFSS. The Fresnel field and the field of the proposed method are calculated through the transmission coefficients. Compared with the far-field pattern, the Fresnel field deteriorates by 1.54 dB in the broadside direction and the first SLL increases by 5.91 dB. The field of the proposed method matches well with the far-field pattern. Fig. 15(b) shows the errors between the patterns in Fig. 15(a). The maximum error of the Fresnel field is 17.40 dB, which occurs at the first null of the far-field pattern. However, the maximum error of the proposed method is only 1.62 dB. Similar to (7), while calculating the errors in Fig. 14(b), the pattern and field are processed as

$$\begin{aligned} F_1' &= \max(F_1, -10\,\text{dBi}) \\ F_2' &= \max(F_2, -10\,\text{dBi}) \\ F_3' &= \max(F_3, -10\,\text{dBi}) \end{aligned} \tag{9}$$

where F_1, F_2, and F_3 are the radiation patterns, obtained from the full-wave simulation. F_1 is the far-field pattern, F_2 is the Fresnel field, and F_3 is the field of the proposed method. Substituting (9) into (8), the errors are obtained as shown in Fig. 15(b).

In practical applications, the phase distribution can be calculated based on the measured distance and element locations of the AUT. Moreover, the phase distribution can be extracted from the phase information as well. According to the proposed method, the phase information can be directly measured. The measurement steps for an N-element antenna array can be summarized as follows.

1) Ensure that the measurement distance R meets the given error criteria as shown in Fig. 13.

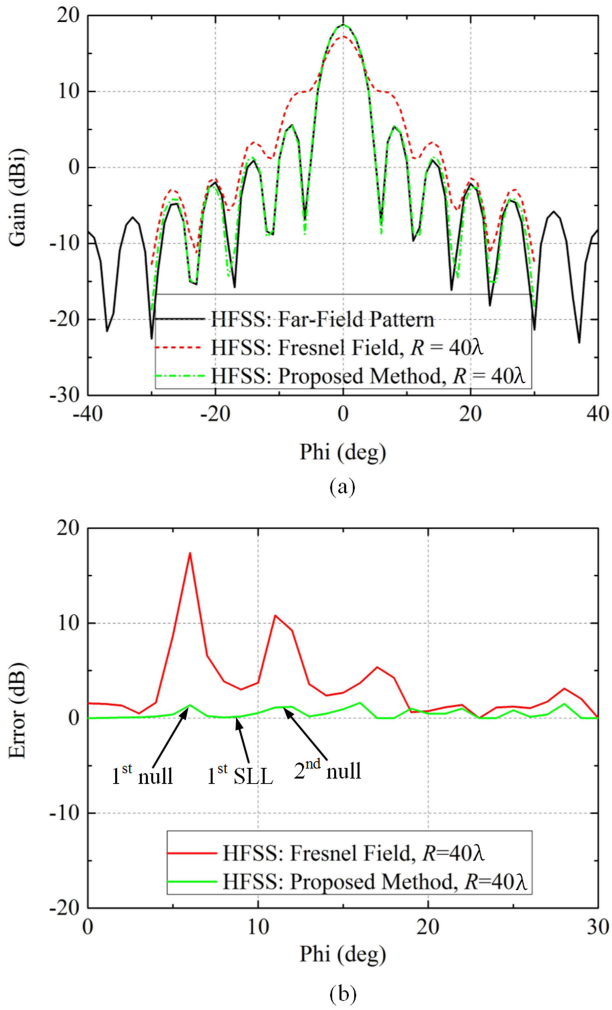

Fig. 15. Full-wave simulation results of the 1-D 20-element array. (a) Simulated patterns of the far-filed pattern, the Fresnel pattern, and the pattern of the proposed method. (b) Errors of the Fresnel pattern and the pattern of the proposed method.

2) Set the source antenna at a distance of R and steer the maximum radiation direction of the AUT toward the source antenna.
3) Use the source antenna to illuminate the AUT and obtain the phase distribution on every antenna element. Assuming the received electric field in the ith radiation element is $E_i = A_i e^{j\beta_i}$ $(i = 1, 2, \ldots, N)$. As a result, the phase distribution is $\beta_i (i = 1, 2, \ldots, N)$.
4) Calculate the conjugation phase of the phase distribution in step 3, i.e., $\beta_i' = -\beta_i$ $(i = 1, 2, \ldots, N)$. The conjugated phase distribution $\beta_i' (i = 1, 2, \ldots, N)$ is the required phase distribution of the proposed method.
5) Excite the AUT with the phase distribution obtained in step 4. The far-field pattern is reconstructed at a distance of R. The directivity pattern can be expressed as

$$D(\theta, \varphi) = \sum_{i=1}^{N} B_i e^{j\psi_i} e^{-j2\pi \frac{r_i}{\lambda}} e^{j\beta'} \tag{10}$$

where B_i and ψ_i are the amplitude and phase distribution of the original array excitation, respectively. $r_i(R, \theta, \varphi)$ is the distance from the ith element to the measurement point, which can be calculated by (5).
6) Rotate the AUT and carry out the pattern measurement as usual.

V. Conclusion

In this paper, a far-field reconstructing method is proposed to reduce the measurement distance of multifeed large-scale antenna arrays. By using this method, the measurement distance can be effectively reduced from the Fraunhofer region to the Fresnel region. In contrast with the previous near-field measurement method, the proposed method directly reconstructs the far-field pattern in the Fresnel region instead of using the NF–FF transformation technique. Compared with the conventional near-field measurement method, the proposed method is less complex and can be easily utilized in normal far-field anechoic chambers, which cannot achieve the Fraunhofer distance of a large-scale antenna array. Both theoretical and full-wave simulations are utilized to validate the proposed method. The simulated results show that the proposed method has high potential for practical applications. It should be noted that the proposed method is only studied and validated for a uniformly spaced point source array. The array is excited in phase or with a progressive phase distribution.

References

[1] E. G. Larsson, O. Edfors, F. Tufvesson, and T. L. Marzetta, "Massive MIMO for next generation wireless systems," *IEEE Commun. Mag.*, vol. 52, no. 2, pp. 186–195, Feb. 2014.
[2] F. Rusek *et al.*, "Scaling up MIMO: Opportunities and challenges with very large arrays," *IEEE Signal Process. Mag.*, vol. 30, no. 1, pp. 40–60, Jan. 2013.
[3] X. Jiang, H. Wang, Z. Zhang, X. Gao, L. Dai, and M. F. Iskander, "Low RF-complexity massive MIMO systems based on vertical spatial filtering for urban macro cellular networks," *IEEE Trans. Veh. Technol.*, vol. 66, no. 10, pp. 9214–9225, Oct. 2017.
[4] C.-M. Chen, V. Volski, L. V. d. Perre, G. A. E. Vandenbosch, and S. Pollin, "Finite large antenna arrays for massive MIMO: Characterization and system impact," *IEEE Trans. Antennas Propag.*, vol. 65, no. 12, pp. 6712–6720, Dec. 2017.
[5] P. Liu, Z. Zhang, Y. Li, and Z. Feng, "A dual-beam eight-element antenna array with compact CPWG crossover structure," *IEEE Antennas Wireless Propag. Lett.*, vol. 7, pp. 1269–1272, 2017.
[6] M. N. Abdallah, T. K. Sarkar, M. Salazar-Palma, and V. Monebhurrun, "Where does the far field of an antenna start?" *IEEE Antennas Propag. Mag.*, vol. 58, no. 5, pp. 115–124, Oct. 2016.
[7] A. D. Yaghjian, "An overview of near-field antenna measurements," *IEEE Trans. Antennas Propag.*, vol. 34, no. 1, pp. 30–45, Jan. 1986.
[8] IEEE Recommended Practice for Near-Field Antenna Measurements, IEEE Standard 1720-2012, Dec. 2012.
[9] N. Whitelonis, S.-T. Yang, and H. Ling, "Application of near-field to far-field transformation to Doppler features from wind turbine scattering," *IEEE Trans. Antennas Propag.*, vol. 60, no. 3, pp. 1660–1665, Mar. 2012.
[10] C.-C. Oetting and L. Klinkenbusch, "Near-to-far-field transformation by a time-domain spherical-multipole analysis," *IEEE Trans. Antennas Propag.*, vol. 53, no. 6, pp. 2054–2063, Jun. 2005.
[11] E. B. Joy, W. M. Leach Jr., G. P. Rodrigue, and D. T. Paris, "Application of probe-compensated near-field measurements," *IEEE Trans. Antennas Propag.*, vol. AP-26, no. 3, pp. 379–389, May 1978.
[12] Y. Rahmat-Samii, V. G. Israel, and R. Mittra, "A plane-polar approach for far-field construction from near-field measurements," *IEEE Trans. Antennas Propag.*, vol. AP-28, no. 2, pp. 216–230, Mar. 1980.
[13] M. S. Gatti and Y. Rahmat-Samii, "FFT applications to plane-polar near-field antenna measurements," *IEEE Trans. Antennas Propag.*, vol. 36, no. 6, pp. 781–791, Jun. 1988.

[14] F. D'Agostino, F. Ferrara, C. Gennarelli, R. Guerriero, and M. Migliozzi, "Far-field pattern reconstruction from a nonredundant plane-polar near-field sampling arrangement: Experimental testing," *IEEE Antennas Wireless Propag. Lett.*, vol. 15, pp. 1345–1348, 2016.
[15] L. I. Williams, Y. Rahmat-Samii, and R. G. Yaccarino, "The bi-polar planar near-field measurement technique, Part I: Implementation and measurement comparisons," *IEEE Trans. Antennas Propag.*, vol. 42, no. 2, pp. 184–195, Feb. 1994.
[16] R. G. Yaccarino, Y. Rahmat-Samii, and L. I. Williams, "The bi-polar near-field measurement technique, Part II: Near-field to far-field transformation and holographic imaging methods," *IEEE Trans. Antennas Propag.*, vol. 42, no. 2, pp. 196–204, Feb. 1994.
[17] F. D'Agostino, F. Ferrara, C. Gennarelli, R. Guerriero, and M. Migliozzi, "Fast and accurate far-field prediction by using a reduced number of bipolar measurements," *IEEE Antennas Wireless Propag. Lett.*, vol. 16, pp. 2939–2942, 2017.
[18] S.-S. Oh, J.-M. Kim, J.-H. Yun, and S.-Y. Kang, "Antenna measurement method in Fresnel region by ϕ-variation scanning," *IEEE Antennas Wireless Propag. Lett.*, vol. 7, pp. 206–209, 2008.
[19] F. D'Agostino, F. Ferrara, C. Gennarelli, R. Guerriero, and M. Migliozzi, "An effective NF-FF transformation technique with planar spiral scanning tailored for quasi-planar antennas," *IEEE Trans. Antennas Propag.*, vol. 56, no. 9, pp. 2981–2987, Sep. 2008.
[20] F. D'Agostino, F. Ferrara, C. Gennarelli, R. Guerriero, S. McBride, and M. Migliozzi, "Fast and accurate antenna pattern evaluation from near-field data acquired via planar spiral scanning," *IEEE Trans. Antennas Propag.*, vol. 64, no. 8, pp. 3450–3458, Aug. 2016.
[21] A. Shlivinski and A. Boag, "Multilevel surface decomposition algorithm for rapid evaluation of transient near-field to far-field transforms," *IEEE Trans. Antennas Propag.*, vol. 57, no. 1, pp. 188–195, Jan. 2009.
[22] H.-T. Chou, P. H. Pathak, S.-C. Tuan, and R. J. Burkholder, "A novel far-field transformation via complex source beams for antenna near-field measurements on arbitrary surfaces," *IEEE Trans. Antennas Propag.*, vol. 65, no. 12, pp. 7266–7279, Dec. 2017.
[23] A. G. Toshev, "Application of Fourier integrals for determination of antenna far-field patterns from measurements at Fresnel distances," *IEEE Trans. Antennas Propag.*, vol. 65, no. 4, pp. 1700–1705, Apr. 2017.
[24] S.-S. Oh and J.-H. Yun, "New method for predicting the electromagnetic field at a finite distance using Fresnel field transformation," *IEEE Antennas Wireless Propag. Lett.*, vol. 7, pp. 291–294, 2008.
[25] A. Paulus, J. Knapp, and T. F. Eibert, "Phaseless near-field far-field transformation utilizing combinations of probe signals," *IEEE Trans. Antennas Propag.*, vol. 65, no. 10, pp. 5492–5502, Oct. 2017.
[26] A. Taaghol and T. K. Sarkar, "Near-field to near/far-field transformation for arbitrary near-field geometry, utilizing an equivalent magnetic current," *IEEE Trans. Electromagn. Compat.*, vol. 38, no. 3, pp. 536–541, Mar. 1996.
[27] P. Petre and T. K. Sarkar, "Planar near-field to far-field transformation using an array of dipole probes," *IEEE Trans. Antennas Propag.*, vol. 42, no. 4, pp. 534–537, Apr. 1994.
[28] F. Las-Heras and T. K. Sarkar, "A direct optimization approach for source reconstruction and NF–FF transformation using amplitude-only data," *IEEE Trans. Antennas Propag.*, vol. 50, no. 4, pp. 500–510, Apr. 2002.
[29] R. Maaskant, M. V. Ivashina, S. J. Wijnholds, and K. F. Warnick, "Efficient prediction of array element patterns using physics-based expansions and a single far-field measurement," *IEEE Trans. Antennas Propag.*, vol. 60, no. 8, pp. 3614–3621, Aug. 2012.
[30] C. A. Balanis, *Antenna Theory: Analysis and Design*, 3rd ed. Hoboken, NJ, USA: Wiley, pp. 331–333.

Peiqin Liu (S'17) received the B.S. degree from the University of Electronic Science and Technology of China, Chengdu, China, in 2014. He is currently working toward the Ph.D. degree in electrical engineering with Tsinghua University, Beijing, China.

His current research interests include antenna design and theory, particularly in antenna arrays based on leaky-wave antenna, massive MIMO antenna array, and millimeter-wave antenna array.

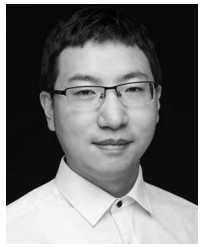

Yue Li (S'11–M'12–SM'17) received the B.S. degree in telecommunication engineering from Zhejiang University, Zhejiang, China, in 2007, and the Ph.D. degree in electronic engineering from Tsinghua University, Beijing, China, in 2012. In December 2013, he was a Research Scholar with the Department of Electrical and Systems Engineering, University of Pennsylvania, Philadelphia, PA, USA. He was also a visiting scholar with the Institute for Infocomm Research (I2R), A*STAR, Singapore, in 2010, and the Hawaii Center of Advanced Communication, University of Hawaii at Manoa, Honolulu, HI, USA, in 2012.

In June 2012, he was a Postdoctoral Fellow with the Department of Electronic Engineering, Tsinghua University. He is currently an Associate Professor with the Department of Electronic Engineering at Tsinghua University, Beijing, China. He has authored or coauthored more than 100 journals and 45 international conference papers, and holds 15 granted Chinese patents. His current research interests include metamaterials, plasmonics, electromagnetics, nanocircuits, mobile and handset antennas, MIMO and diversity antennas, and millimeter-wave antennas and arrays.

He was the recipient of the Issac Koga Gold Medal from URSI General Assembly in 2017; the Second Prize of Science and Technology Award of China Institute of Communications in 2017; the Young Scientist Awards from the conferences of ACES 2018, AT-RASC 2018, AP-RASC 2016, EMTS 2016, and URSI GASS 2014; and the Best Paper Awards from the conferences of CSQRWC 2018, NCMMW 2018 and 2017, APCAP 2017, NCANT 2017, ISAPE 2016, and ICMMT 2016. He was also the recipient of the Outstanding Doctoral Dissertation of Beijing Municipality in 2013 and the Principal Scholarship of Tsinghua University in 2011. He is currently serving as the Associate Editor of IEEE TRANSACTIONS ON ANTENNAS AND PROPAGATION, IEEE ANTENNAS AND WIRELESS PROPAGATION LETTERS, and *Computer Applications in Engineering Education;* and is also in the Editorial Board of *Scientific Report.*

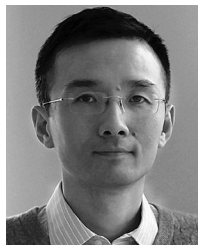

Zhijun Zhang (M'00–SM'04–F'15) received the B.S. and M.S. degrees from the University of Electronic Science and Technology of China, Chengdu, China, in 1992 and 1995, respectively, and the Ph.D. degree from Tsinghua University, Beijing, China, in 1999.

In 1999, he was a Postdoctoral Fellow with the Department of Electrical Engineering, University of Utah, Salt Lake City, UT, USA, where he was appointed as a Research Assistant Professor in 2001. In May 2002, he was an Assistant Researcher with the University of Hawaii at Manoa, Honolulu, HI, USA. In November 2002, he joined Amphenol T&M Antennas, Vernon Hills, IL, as a Senior Staff Antenna Development Engineer and was then promoted to the position of Antenna Engineer Manager. In 2004, he joined Nokia Inc., San Diego, CA, USA, as a Senior Antenna Design Engineer. In 2006, he joined Apple Inc., Cupertino, CA, USA, as a Senior Antenna Design Engineer and was then promoted to the position of Principal Antenna Engineer. Since August 2007, he has been with Tsinghua University, Beijing, China, where he is currently a Professor with the Department of Electronic Engineering. He is the author of the *Antenna Design for Mobile Devices* (Wiley, 1st ed. 2011; 2nd ed. 2017). He served as an Associate Editor of the IEEE TRANSACTIONS ON ANTENNAS AND PROPAGATION (2010–2014) and the IEEE ANTENNAS AND WIRELESS PROPAGATION LETTERS (2009–2015).